RESEARCH ARTICLE | MAY 03 2024

Quantifying wake dynamics subjected to stream vegetation patch elongation: The influence of patch-edge vortices ⊘

Yuan-Heng Zhang (张远恒) ⓘ ; Huan-Feng Duan (段焕丰) ✉ ⓘ ; Xu-Feng Yan (闫旭峰);
Alessandro Stocchino ⓘ

Check for updates

View Online

Export Citation

Articles You May Be Interested In

Three-dimensional flow structures through submerged vegetation patches with uniform and non-uniform stem spacing in an open channel

Physics of Fluids (July 2025)

Soil erosion on steep hills with varying vegetation patterns

Physics of Fluids (January 2025)

Flow and plants

Physics of Fluids (November 2024)

28 November 2025 07:49:06

AIP Publishing

Physics of Fluids

Special Topics Open for Submissions

Learn More

AIP Publishing

Quantifying wake dynamics subjected to stream vegetation patch elongation: The influence of patch-edge vortices

View Online   Export Citation   CrossMark

Yuan-Heng Zhang (张远恒),[1] (ID) Huan-Feng Duan (段焕丰),[1,a] (ID) Xu-Feng Yan (闫旭峰),[2] and Alessandro Stocchino[1] (ID)

AFFILIATIONS

[1]Department of Civil and Environmental Engineering, The Hong Kong Polytechnic University, Hong Kong 999077, China
[2]State Key Laboratory of Hydraulics and Mountain River Engineering, Sichuan University, Chengdu 610065, China

Note: This paper is part of the special topic, Flow and Plants.
[a]Author to whom correspondence should be addressed: hf.duan@polyu.edu.hk

ABSTRACT

Vortices are generated across a wide range of scales due to the interaction between in-stream vegetation and surrounding flows, significantly influencing hydro-geomorphodynamics in earth surface water systems. Recent advance in vegetation patch hydrodynamics has revealed that the elongation of the middle channel patch can generate complex wake flow patterns by adjusting the bleed flow from the patch and triggering the patch-edge Kelvin–Helmholtz (KH) vortices. With a broader range of experimental configurations, this study reveals how the patch wake mixing is apparently strengthened by the presence of KH vortices, indicated by a larger steady wake velocity, a shorter steady wake length, and a damped energy of wake von Karman vortex. Furthermore, we quantify these characteristic metrics of patch wake behavior with and without the influence of KH vortices. Our findings provide insights into the role of vegetation-induced vortex interactions in regulating mixing processes, thereby promoting informed practices in environmental flows.

Published under an exclusive license by AIP Publishing. https://doi.org/10.1063/5.0204290

I. INTRODUCTION

Vegetation plays an important role in aquatic ecosystems. It provides shelter and habitat for living organisms, protects coastal and riverbank regions from waves, currents, and floods, and enhances water quality by filtering nutrients. To protect vegetation habitats and improve restoration efforts, understanding flow-vegetation dynamics is of paramount importance and will lead to more accurate models of sediment transport,[1,2] landscape evolution, and water quality management. Vegetation patches with finite lengths (L) and widths (W) are prevalent in aquatic ecosystems and fluvial environments.[3] Due to the blockage effect of vegetation patch, flow diversion is observed upstream and within the patch (Fig. 1), increasing the flow in the free stream regions and reducing the flow within and behind the vegetation patch.[4,5] For an emergent vegetation patch, the Kelvin–Helmholtz (KH) coherent structure may be triggered at the lateral edge of the patch under sufficiently strong velocity shear,[4,6] restricting the patch lateral extension.[7–11] Bleed flow, which refers to the flow through the patch,[12,13] produces a steady wake region with low velocity and turbulence downstream the patch, facilitating the sediment deposition[14] and patch elongation in the streamwise direction.[15–17] After the steady wake region, a von Karman (VK) vortex street forms, which dramatically amplifies the turbulent intensity thus causing velocity recovery (Fig. 1).

From the perspective of flow adjustment, patch density controls the intensity of local hydraulic resistance; thus, a larger patch density results in a more rapid velocity decrease. Patch dimensions (i.e., L and W) indicate the domain affected by the vegetation-induced resistance, altering the flow structure by accumulating the local flow adjustment as the fluids flow through. Compared to a circular vegetation patch ($L/W = 1$),[13,19] the streamwise velocity within the patch may continue to decrease as the patch elongates downstream (i.e., $L > W$), until reaching equilibrium. The spanwise dimension (W) characterizes the distance for flow deflection into the patch lateral bare regions; thus, a larger W may lead to a weaker flow diversion and further a slower velocity adjustment.[4] Thereby, taking into account the influence of L and W on interior flow adjustment, the patch aspect ratio (L/W) is combined with patch density, represented by the solid volume fraction [$\Phi = N\pi d^2/4$, where $N(\mathrm{m}^{-2})$ is the number of rods per unit bed area, d is the rod diameter], to define the cumulative hydraulic resistance, namely, $\Phi L/W$.[18]
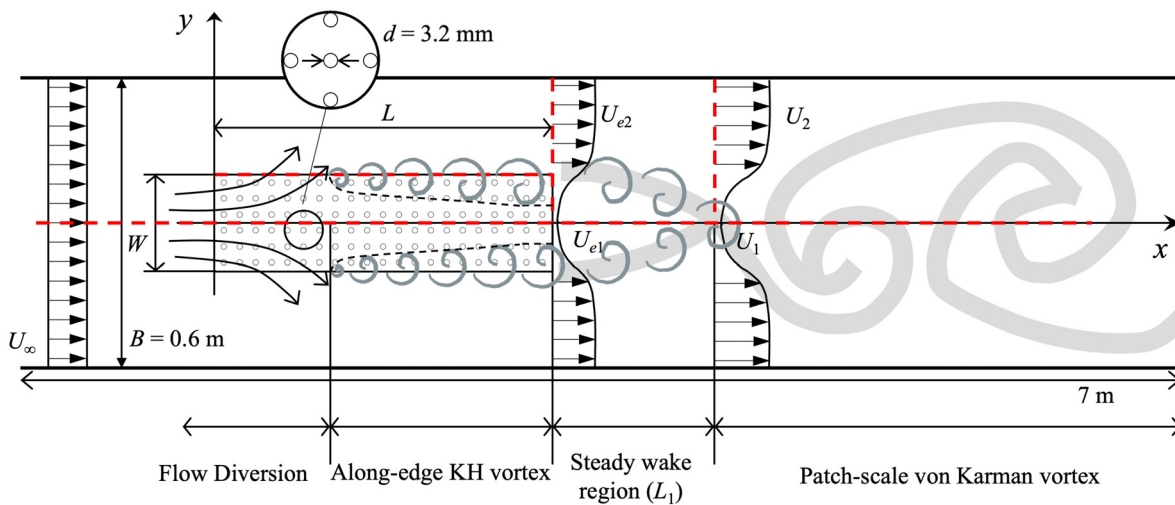
28 November 2025 07:49:06

FIG. 1. Flow structure within and around the rectangular vegetation patch. Patch configuration and longitudinal and lateral transects (red dashed lines) of velocity measurements from top view as adapted from Ref. 18.

According to previous studies of mixing layers in compound channels and partially obstructed channels, KH vortex may be detected when the velocity shear across the lateral interface $\lambda = (U_{y2} - U_{y1})/(U_{y2} + U_{y1}) \geq 0.3$, where U_{y2} is the velocity of the high-speed ambient stream at the interested transect and U_{y1} is the velocity of the low-speed ambient stream at the same transect.[6,20–22] In addition, the patch-scale VK vortex after a finite patch can be triggered under sufficient velocity deficit in the bleed flow from the patch, $(L/W)(U_{e2} - U_{e1})/U_\infty > 0.55$, where U_{e1} is the velocity at the middle of the patch trailing edge and U_{e2} is the constant velocity at the lateral bare region at the same transect.[5,18] However, the patch-edge KH and patch-wake VK vortex were usually studied separately in the literature. Limited studies focused on their dynamic interaction mechanism when they appear simultaneously. Our recent study[18] has indicated the simultaneous formation of both patch-edge KH vortices and patch-wake VK vortices around an elongated rectangular patch and revealed the tendency of the same frequency evolution of the two patterns of vortices. However, the information provided in our previous work[18] is not sufficient to evaluate how the patch-edge KH vortices affect the wake flows. Herein, this study aims to further extend this research direction of Ref. 18 and quantify the influence of patch-edge KH vortices on the patch-wake structure. The main objectives of this paper are:

(1) to investigate the relationship between the cumulative hydraulic resistance and the velocity adjustment at the end of the patch;
(2) to characterize patch-edge KH vortex at a patch with finite width and length and to quantify its effect on the patch-wake structure.

II. MATERIALS AND METHODS

Wake structure is significantly affected by the bleed flow velocity adjusted by vegetation patch, including vegetation density and patch dimensions. Meanwhile, patch elongation enhances cross-stream velocity gradient and triggers the patch-edge KH vortex. To further investigate the impact of patch-edge KH vortex on the wake flows,

wake flows after patches with and without KH vortex generated were compared under various bleed flow adjustment. Therefore, this experiment extends our previous work[18] by testing cases with a wider range of patch length and density to create more wake patterns and comparable conditions. The details of the experiment set up are described as followed.

The experiments were conducted in a laboratory flume with a test section that had a width (B) of 0.6 m, a length of 7 m, and a slope of 1/1000. Plants were simulated with circular perforated polyvinyl chloride (PVC) rods of a diameter $d = 3.2$ mm, which were held in an aligned pattern by perforated PVC baseboards covering the entire test section bottom. The patches were emergent and centrally located in the flume. The leading edge of the patch was located at 1.5 m downstream of the channel inlet, where the flow has been verified to be fully developed. The experiments covered six patch densities, represented by solid volume fractions, of $\Phi = N\pi d^2/4 = 0.007 - 0.080$, where $N(\mathrm{m}^{-2})$ is the number of rods per unit bed area. The corresponding frontal area per unit volume was $a = Nd = 2.8 \sim 31.9\,\mathrm{m}^{-1}$. Various patch lengths of $L = 0.1$–2.0 m, and two patch widths of $W = 0.09, 0.21$ m were employed, leading to a wide range of aspect ratios, $L/W = 0.47$–22.22. A total of 46 patch configurations were tested and analyzed along with 19 experiment runs from Ref. 18. Detailed information for each case is presented in the supplementary material. For hydraulic conditions, the water level was fixed at $h = 22.0 \pm 0.2$ cm and the incoming velocity kept constant to be $U_\infty = 8.0 \pm 5\%$ cm/s. The Froude number $[Fr = U_\infty/(gh)^{1/2}]$ and the Reynolds number ($Re = U_\infty h/\nu$, where ν is the kinematic viscosity of the water, $\nu = 10^{-6}\mathrm{m}^2/\mathrm{s}$), were 0.05 and 17 600, respectively, so that the flow was sub-critical and turbulent. Based on a careful experimental verification,[18] vortex initiation would not be affected by the bottom friction and sidewall effect in the present experiments.

Velocities were measured by a 3D Nortek Vectrino Profiler (acoustic Doppler velocimeter, ADV). Velocities within 40–60 mm from the down-looking probe were collected. For each point, velocity was collected with a sampling time of 120 s and a sampling rate of

75 Hz, which has been verified to be sufficient to capture the flow characteristics in the current experimental setting.[18] Within the patch, velocities were collected in the middle between the cylinders to mitigate stem-scale disturbance and heterogeneity. Only horizontal components measured at mid water depth ($h/2$) have been used to represent the two-dimensional flow structure within and around an emergent patch following Ref. 5. The origin of the Cartesian coordinate system was placed in the middle of the leading edge of the patch as $x = 0$ at the leading edge of the array, positive downstream; $y = 0$ at the channel centerline (Fig. 1). The velocity components were denoted as u, v in the x, y directions, respectively. To evaluate the flow development and coherent structures, velocities along the patch centerline ($y = 0$) and along the patch side edge ($y = W/2$) were measured. To characterize the wake structure, the flow adjustment at the start and end of the steady wake region ($x = L$ and $x = L + L_1$) was evaluated. The lateral measurements were only conducted in one half ($y = 0 - B/2$) of the flume due to symmetric configuration. The transects of velocity measurements were denoted by the red dashed lines in Fig. 1. For velocity and turbulence analysis, raw ADV data with a correlation coefficient of less than 70% was prefiltered. The spikes from ADV measurements were removed by the method developed by Goring,[23] which is widely applied in vegetated flows.[24,25] Each velocity record was decomposed into time-averaged components (U, V) and fluctuating components (u', v'). To qualify the two-dimensional turbulent characteristics, the power spectral density (S_{vv}) and autocorrelation function (R_{vv}) of the cross-stream velocity (v), time-averaged Reynolds shear stress, $-\overline{u'v'}$, were evaluated. S_{vv} were calculated by Welch's method[26] with a Hamming window of equal size of 40 s and a 50% overlap. The formation and strength of the coherent structures can be characterized by the peaks in S_{vv}[27,28] and the oscillations in R_{vv}.[29]

Based on the aforementioned flow measurements, characteristic metrics (see Fig. 1) in vegetation patch flows can be provided. The steady wake length, L_1, is estimated from the longitudinal velocity profile as the distance from the downstream end of the patch to the position where the velocity begins to increase. U_1 is the velocity at $x = L + L_1$, $y = 0$ and U_2 is the velocity of the high-speed ambient flow at the corresponding x transect, i.e., $x = L + L_1$. Similarly, U_{e1} is the velocity at the central point of the patch trailing edge, and U_{e2} is

defined as the velocity at the bare region at the same transect, i.e., $x = L$. The turbulence energy associated with patch-wake coherent structure is characterized by $(U_2 - U_1)^2$. All velocities defined here were time-averaged and measured at the middle of the water height (Fig. 1). These characteristic metrics represent how the patch-edge KH vortices influence the flow structure dominated by the patch-wake VK vortices quantitatively. All these measured data are listed in the supplementary material.

III. RESULTS AND DISCUSSION

A. Bleed flow deficit related to cumulative hydraulic resistance

Threshold values related to bleed flow deficit, $(L/W)(U_{e2} - U_{e1})/U_\infty$, and patch cumulative hydraulic resistance, $\Phi L/W$, have been recently developed to predict the initiation of wake vortex.[18] Specially, flow adjustment at the end of the patch is highly dependent on the patch cumulative hydraulic resistance, but $(L/W)(U_{e2} - U_{e1})/U_\infty$ is not exactly equivalent to $\Phi L/W$, with different performances under the variation of patch density and aspect ratio. Under the same aspect ratio [Fig. 2(a)], the bleed flow velocity deficit is initially positively associated with patch density and finally achieves equilibrium, implying full adjustment of the interior flow before the end of the patch. Increasing the patch density accelerates the interior flow adjustment, resulting in a shorter adjustment length. After the interior adjustment, the flow diversion diminishes, leading to a constant velocity difference at the end of the patch ($(U_{e2} - U_{e1})/U_\infty$), as indicated in Fig. 2(a). Therefore, it is assumed,

$$(U_{e2} - U_{e1})/U_\infty \propto (\Phi)^{-1}. \tag{1}$$

Under the same patch density and patch width that dominate the streamwise gradient of interior flow adjustment,[4,18] $(U_{e2} - U_{e1})/U_\infty$ is proportional to L/W before the full development of the flow within the patch, behaving like patch density [Fig. 2(b)]. Therefore,

$$(U_{e2} - U_{e1})/U_\infty \propto (L/W)^{-1}. \tag{2}$$

Here, considered that the bleed flow adjustment is a result of the combined contributions from patch density and aspect ratio, it is assumed,
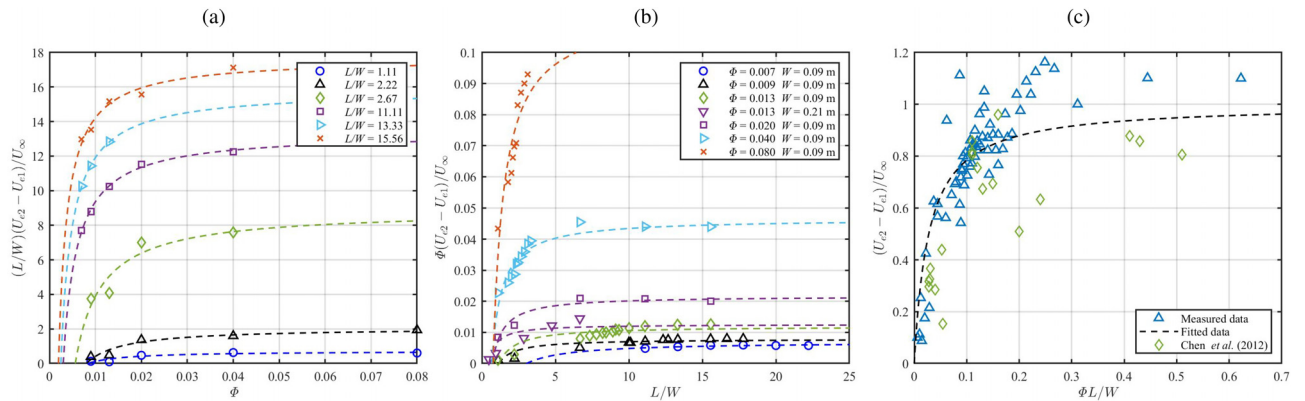

FIG. 2. The relationship between the bleed flow adjustment, $(U_{e2} - U_{e1})/U_\infty$, and (a) patch density, Φ, shifted by L/W for clarity; (b) patch aspect ratio, L/W, shifted by Φ for clarity. The dashed lines with corresponding color for each case indicate the general trend of the measured data. (c) The relationship between $(U_{e2} - U_{e1})/U_\infty$ and cumulative hydraulic resistance, $\Phi L/W$. The dashed line indicates Eq. (5), with a coefficient of determination, $R^2 = 0.75$.

$$(U_{e2} - U_{e1})/U_{\infty} = k - c_1/(\Phi L/W + c_2), \tag{3}$$

where k, c_1, c_2 are the scaling factors to meet the extreme conditions and ensure the equation's validity. For instance, for an extremely high-density porous patch like a solid obstruction or an elongated patch with an interior velocity decay to zero,[4] $\Phi L/W \gg c_1$, $U_{e1} \approx 0$ and $U_{e2} \approx U_{\infty}$, then $(U_{e2} - U_{e1})/U_{\infty} = k = 1$; for an extremely low-density porous patch like none of obstruction, i.e., $\Phi = 0$, $U_{e2} - U_{e1} = 1 - c_1/c_2 = 0$, thus $c_1 = c_2$. Then,

$$(U_{e2} - U_{e1})/U_{\infty} = 1 - c_1/(\Phi L/W + c_1). \tag{4}$$

By data fitting with all measured data, it is obtained

$$(U_{e2} - U_{e1})/U_{\infty} = 1 - 0.03/(\Phi L/W + 0.03) \tag{5}$$

with a correlation coefficient equal to 0.75 ($R^2 = 0.75$).

Particularly, data related to circular patches (i.e., $L/W = 1$)[13] is also included in Fig. 2(c), demonstrating the generality of the developed formulation (i.e., $L/W = 1$). To conclude, patch cumulative hydraulic resistance, $\Phi L/W$, promotes the velocity difference between the in-patch and lateral-outside-patch regions, until the interior flow fully develops. However, according to the observations in our previous work,[18] in addition to velocity adjustment, patch dimensions should be incorporated [i.e., $(L/W)(U_{e2} - U_{e1})/U_{\infty}$] to include the impact of the presence of patch-scale KH vortex at the patch lateral edges on the wake structures.

B. Patch-edge KH coherent structure

In addition to the wake VK vortex, patch elongation actively contributes to the initiation of KH vortex at the patch lateral interfaces. The initiation and strength of the large-scale coherent structure is identified by the peak in power spectra density (S_{vv}) and oscillations in the autocorrelation (R_{vv}) of the cross-stream velocity series[6] collected at the end of the patch lateral edge ($x = L$, $y = W/2$). The frequency
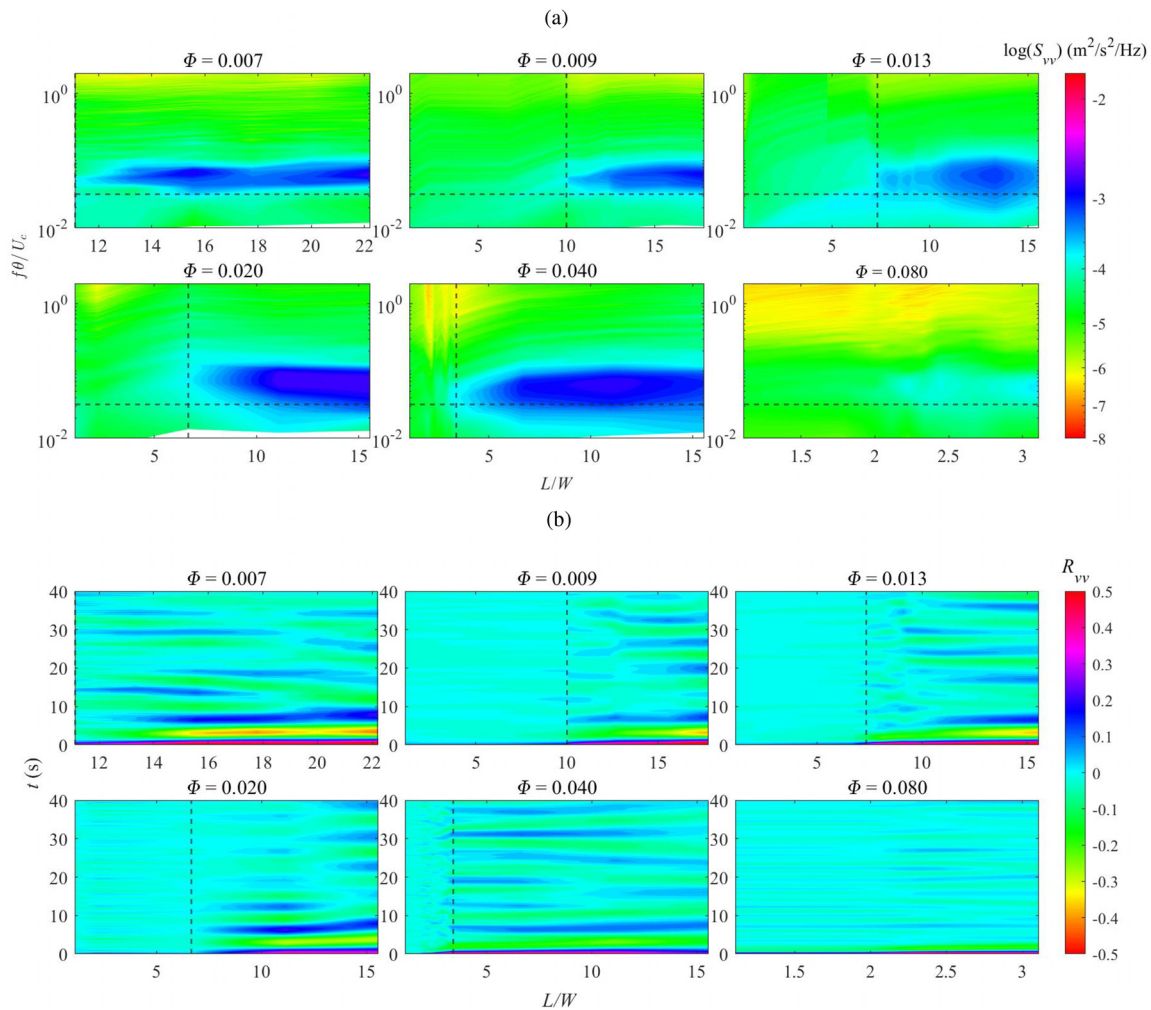

FIG. 3. The initiation and evolution of the patch-scale KH vortex at the end of the patch side edge, i.e., $(x, y) = (L, W/2)$ at different values of L/W under varying Φ, evaluated by the (a) power spectra density (S_{vv}), with a horizontal dashed line indicating the natural frequency for a free shear layer, $f\theta/U = 0.032$; and (b) autocorrelation (R_{vv}) of the spanwise velocity. The vertical dashed line indicates the threshold value of L/W for the initiation of the patch-edge KH vortex.

(f) in S_{vv} is normalized by the local momentum thickness, θ, and convection velocity, U_c, to be $f\theta/U_c$, where $\theta = \int_{-\infty}^{+\infty}[1/4 - ((U - U_c)/\Delta U)^2]dy$, $U_c = (U_{e2} + U_{e1})/2$, and $\Delta U = U_{e2} - U_{e1}$. The spectra manifest a clear peak approximately at $f\theta/U_c = 0.032$, which meets the natural frequency of KH vortices in a plane mixing layer and has been observed in shear layers in partly vegetated flows with both rigid cylinders[30] and flexible vegetation.[6] The results obtained from S_{vv} is consistent with those in R_{vv} (Fig. 3). Similar to the initiation of wake VK vortex,[18] the threshold value of L/W for the KH initiation will be lower under a higher Φ. In addition, the growth and full development of the patch-edge KH vortex are indicated by an initial enhancement and a final equilibrium of the peaks or oscillations in Fig. 3. The weak peaks and small oscillations indicate the generation of small-scale coherent structures in cases with a $\Phi = 0.080$, smaller than the patch-scale coherent structures, which are not considered in the present work.

However, another criterion related to velocity shear (λ-criterion) developed in compound channels or partly vegetated channels[6,22] fails to predict the formation of the patch-scale KH vortex at the patch end [Fig. 4(a)]. Relative to the vortex initiated at a single interface, the interaction of the two KH vortex streets at two parallel streamwise edges across the patch width (W) should be considered in the in-stream located patches, since this communication may enhance the turbulence intensity of the KH vortices.[4] In addition, the λ-criterion was developed from the fully developed transect, but the in-patch flow is not always fully adjusted by the end of the patch investigated in the present work, due to the limited streamwise dimensions. Before fully developed, the in-patch flow keeps diverting into the lateral bare regions, preventing the initiation of the patch-scale coherent structures at the lateral interfaces. For cases with high velocity difference, the patches with low density may have achieved fully developed while the high-density ones may still be in the interior adjustment process. Therefore, the aspect ratio (L/W) is incorporated to consider the extra impacts imposed by the finite dimensions of the patches in the present work, including the interaction of two KH vortex streets across the patch width and the flow diversion due to interior flow adjustment. In Fig. 4(b), patch-edge KH vortex can be detected at the end of the patch when $(L/W)(U_{e2} - U_{e1})/U_\infty > 4.8$, and the turbulent intensity of the KH generally enhances as $(L/W)(U_{e2} - U_{e1})/U_\infty$ increases. Although the magnitude of the velocity difference is relatively small compared to the aspect ratio under an elongated patch, velocity difference is essential in KH vortex generation. For instance, in the partly vegetated flow with sufficient streamwise length, vortex can be triggered once the velocity shear over the threshold value.[6] In a circular or square patch with an aspect ratio $= 1$,[13] $(U_{e2} - U_{e1})/U_\infty$ represents the overall effect of patch density and patch size. Although patch density is not directly presented in this parameter, the impact of which is incorporated in the velocity adjustment.

C. The contribution of the patch-edge KH vortex to wake structure

According to the velocities collected along the patch centerline ($y = 0$), both normalized steady wake length ($L_1/\sqrt{A}$) and steady wake velocity (U_1/U_∞) are suppressed as $\Phi L/W$ increases [Figs. 5(a) and 5(b)], where A refers to the area of the patch, $A = LW$. $\sqrt{A}$ is used to represent the overall size of the rectangular patch, similar to the role of the patch diameter $(D = \sqrt{D^2})$ in the analysis of circular patches with an identical streamwise and spanwise dimension, $L = W = D$.[5,13] The turbulence energy associated with patch-wake coherent structure, $(U_2 - U_1)^2$, is normalized by the energy associated with bed-friction turbulence, $1/2(U_2 + U_1)^2$. The normalized energy of the wake VK vortex is stronger after a patch with a larger value of $\Phi L/W$ [Fig. 5(c)]. However, for circular patches with an aspect ratio $= 1$, the wake flow's behavior varies after patches with the same solid volume fraction but different diameters. The variation of the wake structures under the same value of $\Phi L/W$ [Figs. 5(a)–5(c)] indicates the unequal contributions from Φ and L/W.

Patch aspect ratio affects the wake flow not only by adjusting the bleed flow velocity but also by triggering the KH initiation along the
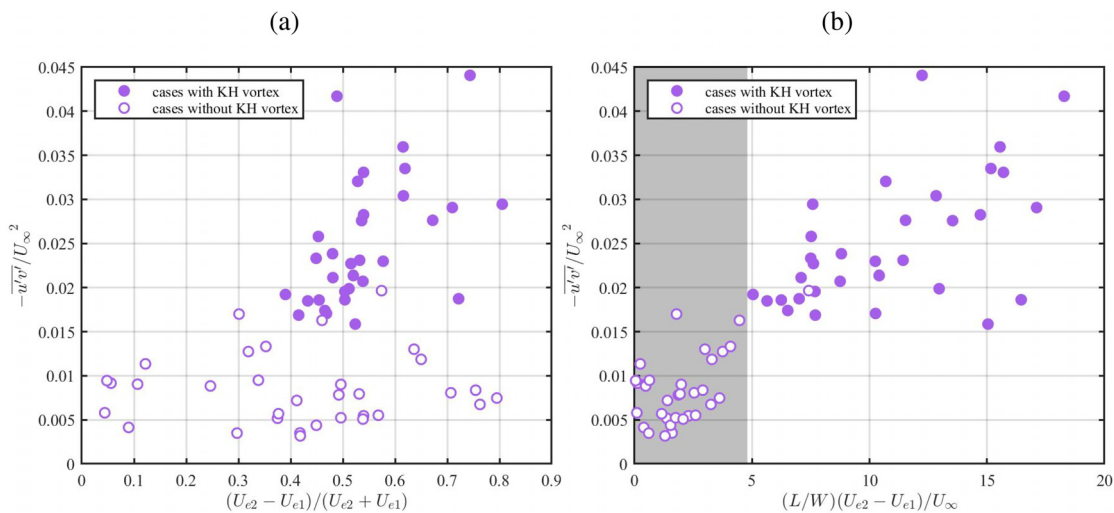
(a)　　　　　　　　　　　　　　　　　　　　(b)

FIG. 4. Indicator for the patch-edge KH vortex initiation and normalized Reynolds stress at the position of $(x, y) = (L, W/2)$: (a) velocity shear, $(U_{e2} - U_{e1})/(U_{e2} + U_{e1})$, and (b) velocity difference along with aspect ratio, $(L/W)(U_{e2} - U_{e1})/U_\infty$.
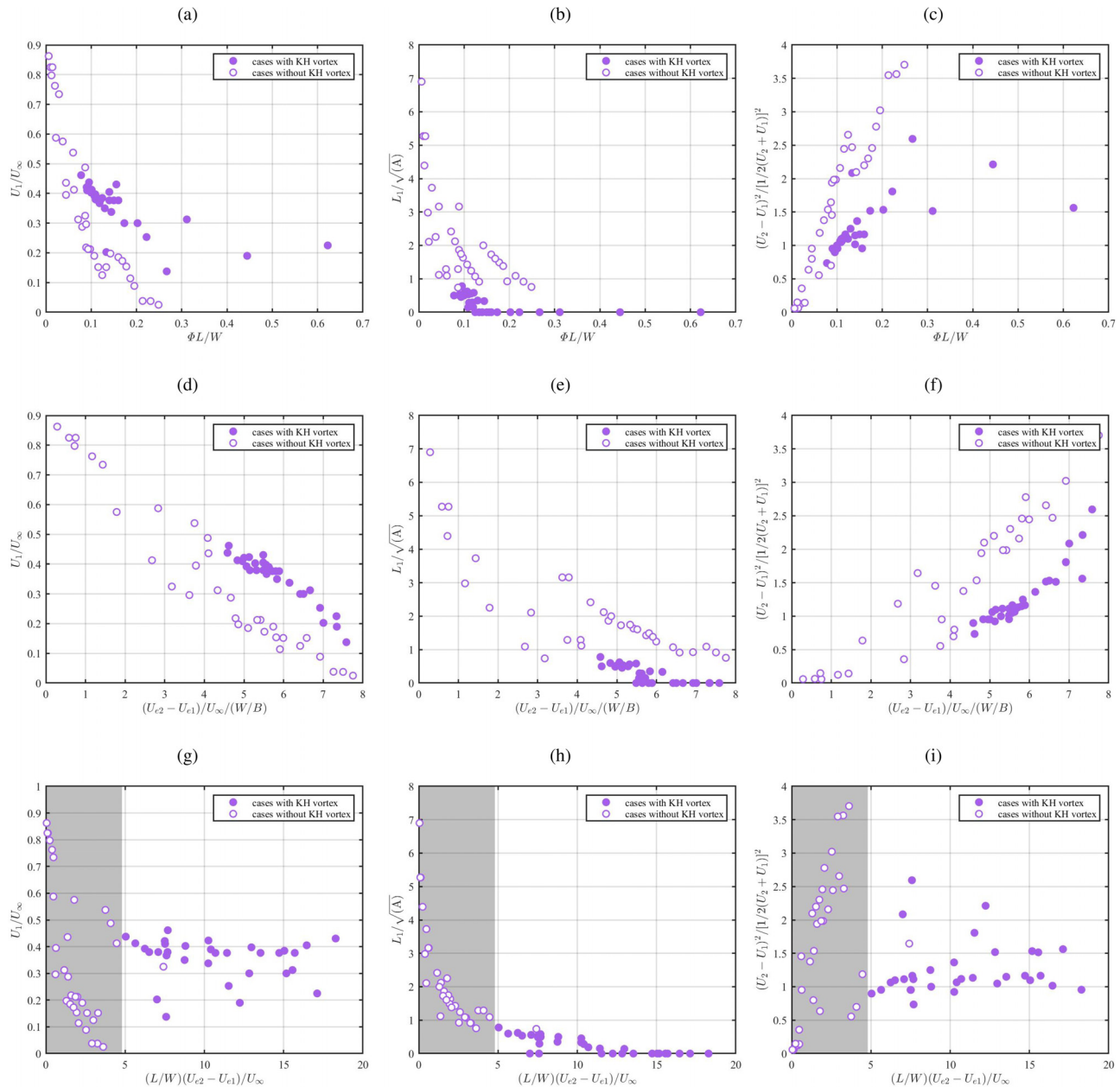
FIG. 5. The impact of the patch-edge KH vortex on (a), (d), and (g) the normalized steady wake velocity, U_1/U_∞, (b), (e), and (h) the normalized steady wake length, $L_1/\sqrt{A}$, and (c), (f), and (i) the normalized energy of the wake vortex, $(U_2 - U_1)^2/[1/2(U_2 + U_1)]^2$.

lateral edges, different from patch density. Thus, it is considered the variations in the wake flow performances are introduced by the presence of the patch-edge KH vortex. However, the influences of bleed flow velocity adjustment and the patch-edge KH vortex generation cannot be simply evaluated by Φ and L/W separately, since patch elongation also makes contributions to modify transverse velocity gradient. To obtain a better understanding of the impact from the initiation of the patch-edge KH vortex, wake structures are compared under the

same normalized transverse velocity gradient obtained at the end of the patch, $(U_{e2} - U_{e1})/U_\infty/(W/B)$, with flume width, B, for normalization. Two distinct trends are detected in the wake structure, with a gap evaluating the contribution of the KH vortex [Figs. 5(d)–5(f)]. Figure 5(e) directly manifests that the generation of the patch-edge KH vortex may decline the steady wake length, implying that the patch-edge KH vortex grows faster than the shear layer thus the mixing point will be closer to the patch trailing edge. Meanwhile, the steady wake

velocities are enhanced compared to the patches without KH vortex [Fig. 5(d)], revealing that the formation of patch-edge KH vortex may accelerate the velocity behind the patch. Furthermore, the normalized energy of the patch-wake VK vortex will be dampened when the upstream KH vortex is generated [Fig. 5(f)]. The enhancement or suppression (i.e., contribution) does not vary with the normalized transverse velocity gradient investigated. Therefore, the results suggest that the presence of the patch-edge KH vortex not only affects the flow condition at the patch lateral interfaces but also presents potential impacts on the wake structure or interacts with the wake vortex.

Indeed, the formation of the patch-scale KH vortex along the patch lateral interfaces induced by patch elongation may introduce extra influences on the wake flow. However, neither cumulative hydraulic resistance nor normalized transverse velocity gradient is a successful indicator for the wake structure since they cannot evaluate the patch-scale KH coherent structure. Given the fairy good performance of $(L/W)(U_{e2} - U_{e1})/U_\infty$ in characterizing the initiation and evolution of the patch-edge KH vortex [Fig. 4(b)], the wake structures can be well predicted by $(L/W)(U_{e2} - U_{e1})/U_\infty$ [Figs. 5(g)–5(i)]. Before the patch-edge KH vortex initiates, i.e., $(L/W)(U_{e2} - U_{e1})/U_\infty < 4.8$, the turbulent intensity is relatively low, thus the transverse velocity gradient dominates the wake structures. Under the above condition, the normalized steady wake length and normalized steady wake velocity drop while the energy of the wake Karman vortex enhances, as bleed flow velocity decays, consistent with the observations from circular patches with no patch-scale KH vortex formation.[5] As $(L/W)(U_{e2} - U_{e1})/U_\infty$ further increases, the patch-edge KH vortex starts to form and grow, disturbing the wake structures. This disturbance of KH vortex on wake flow is also discussed under a submerged circular patch.[19] Although the wake structures behave differently before and after the patch-edge KH vortex occurs, they can be reasonably predicted by $(L/W)(U_{e2} - U_{e1})/U_\infty$, revealing the dominance of the combined effect of the transverse velocity gradient and the presence of KH vortex. Although Φ is not directly presented in this parameter, its influences are incorporated in the velocity difference.

Finally, a phenomenological model can shed light on the understanding of how the patch-wake VK vortex structure responds to the upstream patch-edge KH vortex. Without the KH vortex (e.g., short dense patch), two shear layers at the edge end $(L, \pm W/2)$ grow in parallel and then reattach to form VK vortex structure at the end of the steady wake zone.[5] The self-rotation of the KH vortex structure with high turbulent energy tends to distort the two shear layers, leading to an asymmetrical oscillating steady wake (refer to Fig. 4 in Ref. 18). Furthermore, the fundamental properties of the wake structure are either enhanced (e.g., U_1/U_∞) or weakened {e.g., $L_1/\sqrt{A}$ and $(U_2 - U_1)^2/[1/2(U_2 + U_1)]^2$} by the KH vortex. Comparable phenomenon can be observed in the flow around two tandem square cylinders,[31] where the upstream vortex contributes to suppressing the steady wake region after the downstream cylinder. This phenomenological model also offers some implications for the mathematical description of the co-existence of different vortex structures. In addition, the in-patch velocity recovery after the interior velocity adjustment (i.e., velocity drop) within a rectangular patch,[4,18] can also prove the positive contributions from the KH vortex communication to steady wake velocity.

IV. CONCLUSIONS

This study investigates the relationship between the cumulative hydraulic resistance and bleed flow adjustment, and evaluates the responses of the wake structure to the formation of patch-scale KH vortices along the lateral interfaces of an in-stream located rectangular vegetation patch. By varying patch densities and aspect ratios, it is observed that patch elongation affects the wake structure by adjusting the bleed flow velocity deficit as well as triggering the KH vortex along the patch lateral edges. The initiation of the patch-edge KH vortex at a vegetation patch with finite length and width is highly sensitive to the aspect ratio of the patch, in addition to the velocity difference across the interface. Furthermore, the initiation of the patch-edge KH vortex may accelerate the steady wake velocity, shorten the steady wake length and decay the energy of the wake vortex. Finally, the wake structure can be quantitatively characterized by the combined effect of bleed flow velocity deficit and the initiation of the patch-edge KH vortex. The study improves the understanding of flow-vegetation dynamics and provides critical information on further studies on sediment transport, landscape evolution, and water quality management in vegetated streams, wetlands, estuaries and coastal regions.

SUPPLEMENTARY MATERIAL

See the supplementary material for detailed information on each experimental case.

AUTHOR DECLARATIONS
Conflict of Interest

The authors have no conflicts to disclose.

Author Contributions

Yuanheng Zhang: Formal analysis (equal); Methodology (equal); Writing – original draft (equal). **Huan-Feng Duan:** Funding acquisition (equal); Supervision (equal); Writing – review & editing (equal). **Xufeng Yan:** Conceptualization (equal); Writing – review & editing (equal). **Alessandro Stocchino:** Supervision (equal); Writing – review & editing (equal).

DATA AVAILABILITY

The data that support the findings of this study are available within the article and its supplementary material.

REFERENCES

[1]J. Q. Yang, H. Chung, and H. M. Nepf, "The onset of sediment transport in vegetated channels predicted by turbulent kinetic energy," Geophys. Res. Lett. **43**, 11,261–11,268, https://doi.org/10.1002/2016GL071092 (2016).

[2]Y. Shan, T. Zhao, C. Liu, and H. Nepf, "Turbulence and bed load transport in channels with randomly distributed emergent patches of model vegetation," Geophys. Res. Lett. **47**, e2020GL087055, https://doi.org/10.1029/2020GL087055 (2020).

[3]K. Sand-Jensen and M. L. Pedersen, "Streamlining of plant patches in streams," Freshwater Biol. **53**, 714–726 (2008).

[4]J. T. Rominger and H. M. Nepf, "Flow adjustment and interior flow associated with a rectangular porous obstruction," J. Fluid Mech. **680**, 636–659 (2011).

[5]L. Zong and H. Nepf, "Vortex development behind a finite porous obstruction in a channel," J. Fluid Mech. **691**, 368–391 (2012).

[6]G. Caroppi, K. Västilä, J. Järvelä, P. M. Rowi'Ďski, and M. Giugni, "Turbulence at water-vegetation interface in open channel flow: Experiments with natural-like plants," Adv. Water Resour. **127**, 180–191 (2019).

[7]T. Bouma, L. van Duren, S. Temmerman, T. Claverie, A. Blanco-Garcia, T. Ysebaert, and P. Herman, "Spatial flow and sedimentation patterns within patches of epibenthic structures: Combining field, flume and modelling experiments," Cont. Shelf Res. **27**, 1020–1045 (2007).

[8]S. Temmerman, T. Bouma, J. Van de Koppel, D. Van der Wal, M. De Vries, and P. Herman, "Vegetation causes channel erosion in a tidal landscape," Geology **35**, 631–634 (2007).

[9]S. J. Bennett, W. Wu, C. V. Alonso, and S. S. Y. Wang, "Modeling fluvial response to in-stream woody vegetation: Implications for stream corridor restoration," Earth Surf. Processes Landforms **33**, 890–909 (2008).

[10]E. M. Follett and H. M. Nepf, "Sediment patterns near a model patch of reedy emergent vegetation," Geomorphology **179**, 141–151 (2012).

[11]H. S. Kim, I. Kimura, and Y. Shimizu, "Bed morphological changes around a finite patch of vegetation," Earth Surf. Processes Landforms **40**, 375–388 (2015).

[12]C. J. Wood, "Visualization of an incompressible wake with base bleed," J. Fluid Mech. **29**, 259–272 (1967).

[13]Z. Chen, A. Ortiz, L. Zong, and H. Nepf, "The wake structure behind a porous obstruction and its implications for deposition near a finite patch of emergent vegetation," Water Resour. Res. **48**, W09517, https://doi.org/10.1029/2012WR012224 (2012).

[14]C. Le Bouteiller and J. G. Venditti, "Vegetation-driven morphodynamic adjustments of a sand bed," Geophys. Res. Lett. **41**, 3876–3883, https://doi.org/10.1002/2014GL060155 (2014).

[15]W. Vandenbruwaene, S. Temmerman, T. J. Bouma, P. C. Klaassen, M. B. de Vries, D. P. Callaghan, P. van Steeg, F. Dekker, L. A. van Duren, E. Martini, T. Balke, G. Biermans, J. Schoelynck, and P. Meire, "Flow interaction with dynamic vegetation patches: Implications for biogeomorphic evolution of a tidal landscape," J. Geophys. Res. **116**, F01008, https://doi.org/10.1029/2010JF001788 (2011).

[16]A. Gurnell, "Plants as river system engineers," Earth Surf. Processes Landforms **39**, 4–25 (2014).

[17]A. Przyborowski and A. M. Łoboda, "Identification of coherent structures downstream of patches of aquatic vegetation in a natural environment," J. Hydrol. **596**, 126123 (2021).

[18]Y.-H. Zhang, H.-F. Duan, X.-F. Yan, and A. Stocchino, "Experimental study on the combined effects of patch density and elongation on wake structure behind a rectangular porous patch," J. Fluid Mech. **959**, A36 (2023).

[19]C. Liu, Z. Hu, J. Lei, and H. Nepf, "Vortex structure and sediment deposition in the wake behind a finite patch of model submerged vegetation," J. Hydraul. Eng. **144**, 04017065 (2018).

[20]V. Dupuis, S. Proust, C. Berni, and A. Paquier, "Mixing layer development in compound channel flows with submerged and emergent rigid vegetation over the floodplains," Exp. Fluids **58**, 30 (2017).

[21]S. Proust, J. N. Fernandes, J. B. Leal, N. Rivière, and Y. Peltier, "Mixing layer and coherent structures in compound channel flows: Effects of transverse flow, velocity ratio, and vertical confinement," Water Resour. Res. **53**, 3387–3406, https://doi.org/10.1002/2016WR019873 (2017).

[22]V. Dupuis, L. Schraen, and O. Eiff, "Shear layers in two-stage compound channels investigated with LS-PIV," Exp. Fluids **64**, 24 (2023).

[23]D. G. Goring and V. I. Nikora, "Despiking acoustic Doppler velocimeter data," J. Hydraul. Eng. **128**, 117–126 (2002).

[24]C. Liu and H. Nepf, "Sediment deposition within and around a finite patch of model vegetation over a range of channel velocity," Water Resour. Res. **52**, 600–612, https://doi.org/10.1002/2015WR018249 (2016).

[25]T. Zhao and H. M. Nepf, "Turbulence dictates bedload transport in vegetated channels without dependence on stem diameter and arrangement," Geophys. Res. Lett. **48**, e2021GL095316, https://doi.org/10.1029/2021GL095316 (2021).

[26]P. Welch, "The use of fast Fourier transform for the estimation of power spectra: A method based on time averaging over short, modified periodograms," IEEE Trans. Audio Electroacoust. **15**, 70–73 (1967).

[27]B. L. White and H. M. Nepf, "Shear instability and coherent structures in shallow flow adjacent to a porous layer," J. Fluid Mech. **593**, 1–32 (2007).

[28]X. F. Yan, H. F. Duan, W. H. O. Wai, C. W. Li, and X. K. Wang, "Spatial flow pattern, multi-dimensional vortices, and junction momentum exchange in a partially covered submerged canopy flume," Water Resour. Res. **58**, e2020WR029494, https://doi.org/10.1029/2020WR029494 (2022).

[29]S. H. Truong, W. S. J. Uijttewaal, and M. J. F. Stive, "Exchange processes induced by large horizontal coherent structures in floodplain vegetated channels," Water Resour. Res. **55**, 2014–2032, https://doi.org/10.1029/2018WR022954 (2019).

[30]B. L. White and H. M. Nepf, "A vortex-based model of velocity and shear stress in a partially vegetated shallow channel," Water Resour. Res. **44**, W01412, https://doi.org/10.1029/2006WR005651 (2008).

[31]Q. Shui, C. Duan, D. Wang, and Z. Gu, "New insights into numerical simulations of flow around two tandem square cylinders," AIP Adv. **11**, 045315 (2021).

28 November 2025 07:49:06